A Scenario-classification Hybrid-based Banding Method for Power Transfer Limits of Critical Inter-corridors

Lidong Yi, Maosheng Ding, Jili Wang, Gao Qiu, Fei Xue, Ji'ang Liu, Yuxiong Huang, *Student Member*, *IEEE*, Gengfeng Li, *Member*, *IEEE*, and Junyong Liu, *Member*, *IEEE*

***Abstract*—To secure power system operations, practical dispatches in industries place a steady power transfer limit on critical inter-corridors, rather than high-dimensional and strong nonlinear stability constraints. However, computational complexities lead to over-conservative pre-settings of transfer limit, which further induce undesirable and non-technical congestion of power transfer. To conquer this barrier, a scenario-classification hybrid-based banding method is proposed. A cluster technique is adopted to separate similarities from historical and generated operating condition dataset. With a practical rule, transfer limits are approximated for each operating cluster. Then, toward an interpretable online transfer limit decision, cost-sensitive learning is applied to identify cluster affiliation to assign a transfer limit for a given operation. In this stage, critical variables that affect the transfer limit are also picked out via mean impact value. This enables us to construct low-complexity and dispatcher-friendly rules for fast determination of transfer limit. The numerical case studies on the IEEE 39-bus system and a real-world regional power system in China illustrate the effectiveness and conservativeness of the proposed method.**

***Index Terms*—Transfer limit, transfer capability, power transfer inter-corridor, cluster, cost-sensitive learning, banding, power system operation.**

NOMENCLATURE

A. Sets

$\mathbb{B}$	Set of buses
$\mathbb{C}$	Set of contingencies
$\mathcal{C}$	Set of clustering centers
$\mathbb{D}$	Set of loads
$\mathbb{E}$	Set of historical operations and empirical extreme operations
$\mathbb{E}_j$	Operation set belonging to the j^{th} cluster (or operation set corresponding to the j^{th} transfer limit band)
$\mathbb{G}$	Set of synchronous machines
$\mathbb{J}$	Set of operation clusters (or set of transfer limit bands)
$\mathbb{K}$	Set of power transfer inter-corridors
$\mathbb{L}$	Set of lines
$\mathbb{T}$	Set of dispatch time
$\mathbb{W}$	Set of renewable power plants

B. Parameters/Indices

$\boldsymbol{\mathcal{X}}$	Vector containing power angle and speed of generators
$\boldsymbol{\mathcal{Y}}$	Vector containing bus voltage and phase
τ_c^-, τ_c^+	Time before and at fault clearance
τ, τ_0, τ_{end}	Transient period, start time of transient process, and end time of transient process
Δ	A security upper bound for absolute values of generator angular differences, which is usually set to be 180° or 360° in practice
$\boldsymbol{\phi}$	Structural parameters of neural network applied in mean impact value technique
$\Gamma_{ij,s}$	Transfer limit of the s^{th} inter-corridor involving transmission lines i and j
η_s	Security margin of the s^{th} power transfer inter-corridor
ϵ	A set threshold to ensure safe operation of power transfer inter-corridor

Manuscript received: November 30, 2022; revised: April 27, 2023; accepted: July 23, 2023. Date of CrossCheck: July 23, 2023. Date of online publication: August 24, 2023.

This work was supported in part by State Grid Corporation of China Project "Research on high penetrated renewable energy oriented intelligent identification for curtailment impacts and aid decision-making for promoting consumption in regional power grids" (No. 5108-202135035A-0-0-00).

L. Yi and M. Ding are with State Grid Ningxia Electric Power Co., Ltd., Yinchuan, China, and M. Ding is also with State Grid Ningxia Electric Power Research Institute, Yinchuan, China (e-mail: ild@nw. sgcc. com. cn; dingmaosheng1977@126.com).

J. Wang is with Northwest Branch, State Grid Corporation of China, Xi'an, China (e-mail: wjl8291@163.com).

G. Qiu (corresponding author), J. Liu, and J. Liu are with School of Electrical Engineering , Sichuan University, Chengdu, China (e-mail: qiugscu@scu.edu.cn; ymm_liujiang@163.com; jyliu@scu.edu.cn).

F. Xue is with State Grid Ningxia Electric Power Research Institute Yinchuan, Yinchuan, China (e-mail: tjuxf1010@126.com).

Y. Huang and G. Li are with School of Electrical Engineering, Xi'an Jiaotong University, Xi'an, China (e-mail: yuxionghuang@xjtu. edu. cn; gengfengli@mail.xjtu.edu.cn).

DOI: 10.35833/MPCE.2022.000791

μ_1, μ_2 Penalty weights on equality and inequality constraints of economic dispatch model

G_{ij}, B_{ij} Conductance and susceptance between bus i and bus j

k Number of clusters

m_l Number of neurons in the l^{th} layer

n Number of collected operations/scenarios used for cluster analysis

p Dimension of input, which is formed by power system operating variables

$\boldsymbol{P}_D$, $\boldsymbol{Q}_D$ Active and reactive loads of the D^{th} loading bus

$P_{s,m}$ Transfer limit of the s^{th} inter-corridor, which corresponds to the m^{th} operating cluster

$P_g^{\min}$, $P_g^{\max}$ Lower and upper bounds of active generation of the g^{th} generator

P_i^{Inj}, Q_i^{Inj} Net active and reactive injections at bus i

$\Delta P_g^{\min}$, $\Delta P_g^{\max}$ Lower and upper bounds of ramp rate of the g^{th} generator

$P_{ij,l}^{\min}$, $P_{ij,l}^{\max}$ Lower and upper bounds of active power flow from bus i to bus j corresponding to branch l

P_w^{Fore} Forecasted active output of the w^{th} renewable power plant

$P_w^{\min}, P_w^{\max}$ The minimum and maximum power generations of the w^{th} renewable power plant

$Q_g^{\min}$, $Q_g^{\max}$ Lower and upper bounds of reactive generation of the g^{th} generator

κ Dimension of output (note that it is also the number of inter-corridors, i.e., $\kappa = |\mathbb{K}|$)

v_i Quantity of effect of the i^{th} operating variable on the transfer-limit banding

v_i^{MIV} Mean impact value (MIV) quantity of effect of the i^{th} operating variable effect on transfer-limit banding

v_i^{Endo} Endogenous quantity of effect of the i^{th} operating variable on transfer-limit banding

Y_{ij} Element in row i and column j of the cost-sensitive matrix

Z A normalization factor

C. Variables of Transfer-limit Decision

$\boldsymbol{\delta}$ Vector of power angle of each synchronous generator

$\boldsymbol{\omega}$ Vector of speed of each synchronous generator

$\boldsymbol{V}$ Vector of nodal voltages

$\boldsymbol{\theta}$ Vector of nodal phase angles

$\delta_{j,c,t}$ Power angle of the j^{th} generator at time stamp t during occurrence of contingency c

$\underline{P_{k,is}}, \overline{P_{k,is}}$ The minimum and maximum values of power transfer of the k^{th} inter-corridor over insecurity scenarios

$\underline{P_{k,se}}, \overline{P_{k,se}}$ The minimum and maximum values of power transfer of the k^{th} inter-corridor over security scenarios

$\underline{P_k}, \overline{P_k}$ Lower and upper transfer limits of the k^{th} inter-corridor

$\underline{P_{k,is,j}}, \overline{P_{k,is,j}}$ The minimum and maximum values of power transfer of the k^{th} inter-corridor over insecurity scenarios in the j^{th} cluster

$\underline{P_{k,se,j}}, \overline{P_{k,se,j}}$ The minimum and maximum values of power transfer of the k^{th} inter-corridor over security scenarios in the j^{th} cluster

$P_k(i)$ Transmission power in the i^{th} scenario through the k^{th} inter-corridor ($P_k(i) < 0$ stands for the reverse power flow)

$S_c(i)$ Post-fault security state under contingency c of the i^{th} scenario ($S_c(i) = 0$ denotes that the scenario owns insecurity risk)

D. Variables of Economic Dispatch

$\Gamma_{ij,s}(t)$ Transfer limit of the l^{th} line at dispatch timestamp t

$P_g(t)$ Power generation of the g^{th} generator at dispatch timestamp t

$P_w(t)$ Power generation of the w^{th} renewable power plant at dispatch timestamp t

$\Delta P_w(t)$ Power curtailment of the g^{th} renewable power plant at dispatch timestamp t

$P_{ij,l}(t)$ Power flow through the l^{th} line at dispatch timestamp t, whose sending bus and receiving bus are the i^{th} bus and the j^{th} bus, respectively

I. Introduction

RENEWABLE energy penetrated power systems are principal energy carriers under low-carbon concerns. However, the volatility and uncertainty of renewable energy make power system operating conditions more complex and bring tremendous challenges to efficient operation in critical inter-corridors [1], where dispatchers must always monitor interconnected power transfers and control them within transfer limits [2]. However, the strong nonlinearity and high dimensionality in the determination of the transfer limit cause a significant computational burden; thus, in practice, the limits are typically preset to be conservative values a year ahead. To ensure sufficient security and stability margins, practical computations were performed under the most extreme operating conditions. However, this may lead to over-conservative operations and underutilization of the capacity of the transmission lines. Moreover, the true transfer capabilities are dynamic with varying operations. With a higher penetration of renewable energy, power transfer security features a stronger variability in time. Therefore, an accurate and efficient control method is required for inducing flexible transfer limits.

Thus far, the analysis of critical interconnected power transfer capacity has become a popular research topic. Various algorithms have been presented, and typical physics-

based methods can be classified into four broad categories: repeated power flow (RPF) [3], [4], continuation power flow (CPF) [5], optimal power flow (OPF) [6], and sensitivity-based methods [7], [8]. Both the RPF and CPF determine the power transfer capacities by progressively increasing the interconnected power transfers until any security constraints are violated. These are easier to implement than the other alternatives. However, these methods have several limitations. As shown in [3], the power transfer growth path is defined manually, which means that the search direction for the transfer capacities is subjectively and partially determined, and the most conservative operation is difficult to determine. The OPF develops a mathematical optimization model to depict the transfer capacity calculation, and the model is solved using optimization algorithms [6], [9], [10]. For example, in [10], a transient stability-constrained OPF is used to calculate the total transfer capability of tie lines. Thus, a more global search for extreme operations is enabled, and a more accurate and conservative transfer limit can be found, compared with the RPF and CPF. However, [11] indicates that the OPF is time-consuming and has poor convergence when multi-contingency is considered. To address this issue, sensitivity-based methods have been proposed in [7] and [8]. Such methods apply local linear features to simplify the nonlinear dynamics involved in the transfer limit; thus, they are more efficient and exhibit better convergence than the other methods. However, the accuracy is sacrificed. Notably, a generic challenge for the OPF family is that precise physical modeling is indispensable, which is typically of high dimensionality and complexity for dynamic security verification. In conclusion, none of the aforementioned methods are available for practical power systems involving tremendous dynamic components, particularly when highly penetrated renewables induce time-varying operations.

Ahead of online dispatch, dispatchers typically consider the most conservative among a gathered scenario set of transfer capacities as a fixed transfer limit. However, end-to-end computations from operating conditions/scenarios to transfer capabilities are computationally intensive even though the entire process is executed offline.

Reference [12] shows that traditional physics-based models may not compromise computational efficiency, complexity, and overconservativeness. A new idea upon data-driven techniques has been widely used to provide fast and precise computation of transfer capabilities. For instance, [13] provides a linear regression model for the total transfer capability computation, where second-level efficiency is enabled. Despite data-driven methods enabling real-time transfer limit awareness, research is required on generalizability and engineering applicability, as there is a knowledge gap to prove the scalability, interpretability, conservativeness, and generalizability of a trained data-driven model. From the perspective of engineering, a better alternative is to use data-driven methods to assist power system operations indirectly. Therefore, clustering techniques are preferred for power-engineering applications [14], [15]. In [14], typical operating scenarios and their pivotal patterns are identified using clustering methods. It was concluded that power system operations vary with the season, weather, and events. Previous research highlighted that clustering methods do not directly engage in operating decisions; instead, they attempt to render generalized and reliable patterns to assist decision-making and bridge controllable variables and the concerned dispatch objectives.

Inspired by the analysis, this paper develops a scenario-classification hybrid-based banding method for power transfer limits. Notably, this paper does not deal with end-to-end computations from operating conditions to transfer capabilities; instead, a pragmatic way to determine the transfer limit is studied. Our method clusters numerous historical and generated operating data points to finely partition power systems into multiple typical scenarios or subspaces, each of which has a conservativeness-dominated transfer limit. Then, a cost-sensitive classifier is used to bridge the transfer limit and operating conditions and enable real-time and direct online optimization of the transfer limit. The main advantages of the proposed method are as follows.

1) It fixes the poor convergence and computationally cumbersome nature of traditional impractical methods, but still provides a global search method. Compared with the expertise-based method used in power industries, it enables more precise decisions.

2) By customizing the cluster number, the proposed method enables a degree of freedom that compromises the conservativeness and economy of inter-corridor operations. In addition, to assign transfer limits to each cluster, we bridge the transfer limits and operating conditions such that the transfer limits become controllable and can be optimized to release the power transfer potential of the inter-corridors.

3) By incorporating a classification method with clustering, real-time and direct decisions regarding the transfer limit can be made. This can provide efficient control information for flexibly regulating the transfer limit. Interestingly, no sample imbalance issues exist, because the decision model is built on balanced clustering labels.

For better readability, the key ideas of the traditional and proposed methods for deciding and operating power transfers are compared, as shown in Fig. 1. The traditional method intends to find an overconservative transfer limit set throughout the entire operating space of power systems, resulting in unnecessary curtailment of power transfers. The proposed method first settles massive operating subspaces to characterize the entire space intact, and then finds a conservative transfer limit set for each of the subspaces. Thus, we enable secure operations in each subspace, and the transfer limit increases from the perspective of the global operating space.

II. Key Idea of Proposed Method

A. Traditional Transfer Limit Determination

Transfer capabilities of inter-corridors are constrained by transient stability, $N-1$ security, voltage security, etc. These constraints place a heavy computational burden on the determination of the transfer capability.

However, transfer capabilities are time-varying and operation-dependent indices, and they must be updated along with operations such that a precise security situation and a latent increase in power transfers can be realized.

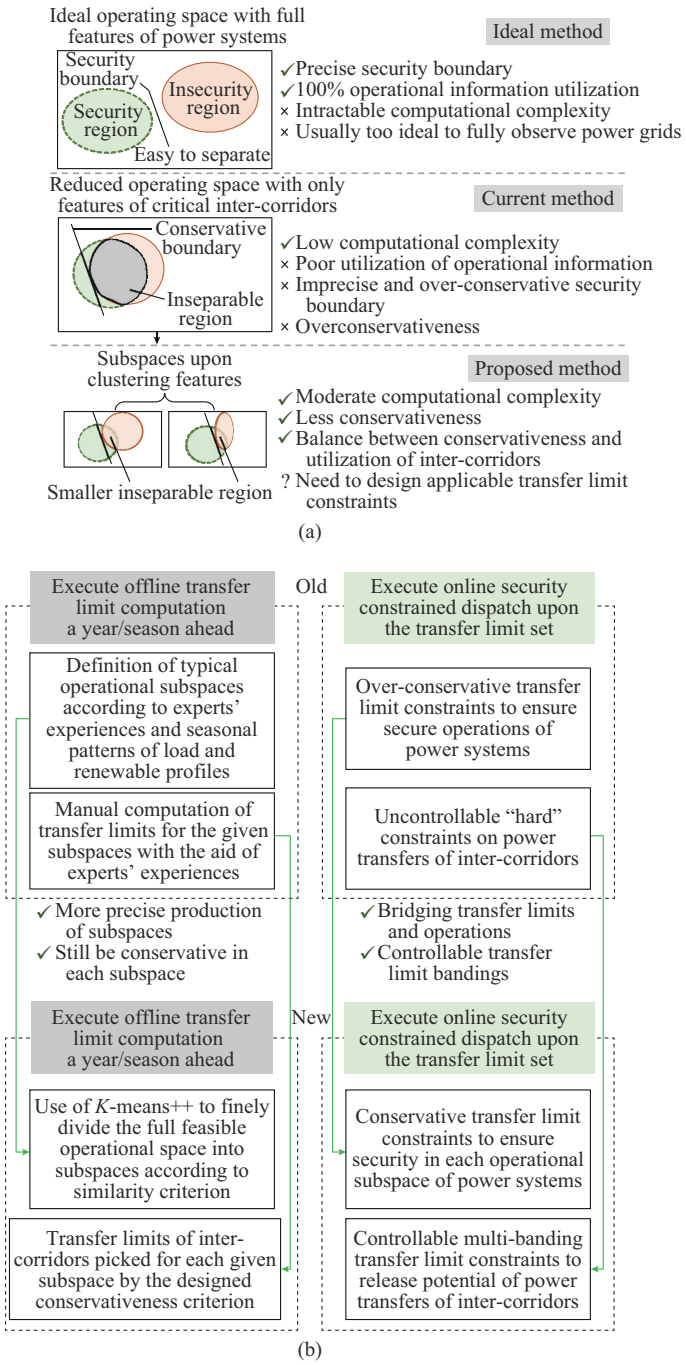

Fig. 1. Intuitive illustrations of contributions of proposed method. (a) Comparisons among ideal method, current method, and proposed method. (b) Key ideas of traditional and proposed methods.

The current research implies a key compromise between precise awareness and fast calculation of transfer capabilities. To solve this issue, dispatchers prefer to conduct fixed transfer limits that come from a conservative operation-mode analysis a year ahead. Figure 2 presents an intuitive illustration of the sketch map of traditional transfer-limit decision method. Because the determination for transfer capability holds nonlinearity and nonconvexity owing to the inclusion of stability constraints, it is unrealistic to determine the transfer capability for each possible operation. Instead, transfer capability computations will only be performed on a few typical operating modes. Among these transfer capabilities, the minimum will be decided as a fixed transfer limit. In the given example, four transfer capacities are calculated, and in practice, dispatchers will set their minimum to deal with online dispatches and constrain power transfer. Therefore, the transfer limit corresponding to the most conservative extreme scenario is picked up, and it implies that, all operations with power transfer larger than this limit will be deemed as insecurity in an online dispatch process. In Fig. 2, the dashed boxes represent the subspaces corresponding to different typical scenarios via clustering techniques, while the solid circles represent the operating conditions in the process of searching for transfer limit.

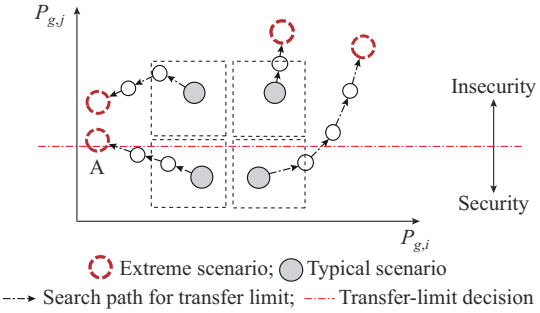

Fig. 2. Sketch map of traditional transfer-limit decision method.

Remark: although the concept of transfer limit appears to be similar to that of transfer capability, there is still a difference. Transfer capability is a dependent variable on operating conditions; thus, it is not pragmatic in a realistic online dispatch because of its time-consuming computation. Instead, dispatchers compute transfer capabilities offline over several empirical extreme scenarios and deploy the most conservative scenario to set a fixed transfer limit on a critical inter-corridor. This process is offline, and in an online dispatch, the security constraints on the inter-corridors are reduced to steady transmission power constraints whose bounds are the determined transfer limits. Therefore, to prevent confusion, we distinguish between the transfer capability and transfer limit, i.e., the transfer capability refers to the true varying power transfer constraint of an inter-corridor, whereas the transfer limit is a constant limit that is set in advance. The latter is a major concern.

As shown in Fig. 2, dispatchers typically start from several typical scenarios to search for the most extreme operating scenarios based on expert experience. This idea is intended to determine the most conservative transfer capability for determining the transfer limit. The lowest power transfer at Point A is selected as the transfer limit. All operations in which the power transfer is below this limit are secure. In addition, because the method is executed offline, the problem of inefficient online calculations is resolved. Because the search for extreme operations is a computationally intensive optimization problem with extremely complicated stability and security constraints, its implementation in real-world power system is difficult. Instead, a more pragmatic method based on the Monte Carlo method is preferred. Suppose that

all historical operations and their search extreme operation scenarios are included in a single operating dataset. The determination of transfer limits in the positive transmission direction is equivalent to finding the smaller value between the minimum power transfer of all insecure operations and the maximum power transfer of secure operations. We can mathematically represent this via (1), where (1a)-(1c) denote the process when the power transfer is in the positive direction, and (1d)-(1f) represent the condition when the power transfer is in the negative direction.

$$\overline{P_k} = \min\left(\overline{P_{k,is}}, \overline{P_{k,se}}\right) \quad \forall k \in \mathbb{K} \tag{1a}$$

$$\begin{cases} \overline{P_{k,is}} = \min\limits_{\forall i \in \mathbb{E}} P_k(i) \\ \text{s.t. } P_k(i) \geq 0 \quad \forall k \in \mathbb{K} \\ \quad\; S_c(i) = 0 \quad \forall c \in \mathbb{C} \end{cases} \tag{1b}$$

$$\begin{cases} \overline{P_{k,se}} = \max\limits_{\forall i \in \mathbb{E}} P_k(i) \\ \text{s.t. } P_k(i) \geq 0 \quad \forall k \in \mathbb{K} \\ \quad\; S_c(i) = 1 \quad \forall c \in \mathbb{C} \end{cases} \tag{1c}$$

$$\underline{P_k} = \max\left(\underline{P_{k,is}}, \underline{P_{k,se}}\right) \quad \forall k \in \mathbb{K} \tag{1d}$$

$$\begin{cases} \underline{P_{k,is}} = \max\limits_{\forall i \in \mathbb{E}} P_k(i) \\ \text{s.t. } P_k(i) < 0 \quad \forall k \in \mathbb{K} \\ \quad\; S_c(i) = 0 \quad \forall c \in \mathbb{C} \end{cases} \tag{1e}$$

$$\begin{cases} \underline{P_{k,se}} = \min\limits_{\forall i \in \mathbb{E}} P_k(i) \\ \text{s.t. } P_k(i) < 0 \quad \forall k \in \mathbb{K} \\ \quad\; S_c(i) = 1 \quad \forall c \in \mathbb{C} \end{cases} \tag{1f}$$

where overline and underline denote power transfer with positive and negative directions, respectively. The security verification, i.e., $S_c(i)$, should embody static, dynamic, and $N-k$ securities. Although our method is compatible with all security validation, only static security, $N-1$ security, and transient angular stability are considered for the sake of simplicity. This enables us to focus on the innovative design of the proposed model. The security verification models are as follows.

$$\begin{cases} \boldsymbol{\mathcal{X}} = [\boldsymbol{\delta}, \boldsymbol{\omega}] \\ \boldsymbol{\mathcal{Y}} = [\boldsymbol{V}, \boldsymbol{\theta}] \end{cases} \tag{2a}$$

$$\begin{cases} \mathbf{0} = \boldsymbol{h}(\boldsymbol{\mathcal{X}}, \boldsymbol{\mathcal{Y}}) \\ \dot{\boldsymbol{\mathcal{X}}} = \boldsymbol{f}_1(\boldsymbol{\mathcal{X}}, \boldsymbol{\mathcal{Y}}) \quad \tau_0 \leq \tau \leq \tau_c^- \\ \dot{\boldsymbol{\mathcal{X}}} = \boldsymbol{f}_2(\boldsymbol{\mathcal{X}}, \boldsymbol{\mathcal{Y}}) \quad \tau_c^+ \leq \tau \leq \tau_{\text{end}} \end{cases} \tag{2b}$$

$$\left\| \delta_{i,c,t} - \delta_{j,c,t} \right\| \leq \Delta \quad \forall i,j \in G, c \in C, t \in \left[\tau_0, \tau_{\text{end}}\right] \tag{2c}$$

where $\boldsymbol{h}(\cdot)$, $\boldsymbol{f}_1(\cdot)$, and $\boldsymbol{f}_2(\cdot)$ represent the power flow equations, differential algebraic equations (DAEs) during and after fault occurrence, respectively. The security criterion is a practical engineering index. It constrains the angle difference between any two generators to be below a predefined threshold, which is typically set to be 180° or 360°. Here we use the 180° criterion. Because massive temporal intermediate variables are introduced, (1) is highly complex. This supports the argument that transfer-limit computation is time-consuming.

After solving (1), we can use (3) to constrain the online dispatches.

$$\underline{P_k} \leq P_k \leq \overline{P_k} \quad k \in \mathbb{K} \tag{3}$$

However, applying the transfer limits determined by conventional method (1) may result in the discarding of some security conditions with high-power transfers. Many security conditions are screened out of the security domain because a nonlinear correlation between power transfers and security conditions jumbles security and insecurity operations near the security boundary. Only sufficiently conservative transfer limits can be determined, which triggers a significant waste of secure operations.

In conclusion, traditional engineering methods undoubtedly lead to overconservative transfer limits such that unnecessary obstruction of power transfer is induced. However, it still offers the advantages of fast online decisions and security guarantees. This paper intends to exploit both traditional engineering methods and existing data-driven methods to meet the demands of practicality and higher availability of inter-corridors.

B. Proposed Banding Method

Over-conservative transfer limits are derived from the elimination of operating domains where security and insecurity conditions coexist. To address this issue, we intend to utilize the unavailable security conditions. Specifically, the proposed solution is to divide the operating scenario set $\mathbb{E}$ into several clusters, followed by the same determination methodology as in (1) to set the transfer limits for each cluster. To produce these clusters, we introduce unsupervised learning (UL). The UL can assemble quantities of similar operating conditions into one cluster and divide the original strong nonlinearity into pieces of linearity or poor nonlinearity, such that there can be a straightforward relationship between power transfers and security in the operating space created by a cluster. In other words, in one cluster, we can approximate a security boundary in the power transfer coordinates. This allows us to determine the transfer limits for each cluster. The specific formulation is given in (4).

$$\overline{P_{k,j}} = \min\left(\overline{P_{k,is,j}}, \overline{P_{k,se,j}}\right) \quad \forall k \in \mathbb{K}, j \in \mathbb{J} \tag{4a}$$

$$\begin{cases} \overline{P_{k,is,j}} = \min\limits_{\forall i \in \mathbb{E}_j, j \in \mathbb{J}} P_k(i) \\ \text{s.t. } P_k(i) \geq 0 \quad \forall k \in \mathbb{K} \\ \quad\; S_c(i) = 0 \quad \forall c \in \mathbb{C} \end{cases} \tag{4b}$$

$$\begin{cases} \overline{P_{k,se,j}} = \max\limits_{\forall i \in \mathbb{E}_j, j \in \mathbb{J}} P_k(i) \\ \text{s.t. } P_k(i) \geq 0 \quad \forall k \in \mathbb{K} \\ \quad\; S_c(i) = 1 \quad \forall c \in \mathbb{C} \end{cases} \tag{4c}$$

$$\underline{P_{k,j}} = \max\left(\underline{P_{k,is,j}}, \underline{P_{k,se,j}}\right) \quad \forall k \in \mathbb{K}, j \in \mathbb{J} \tag{4d}$$

$$\begin{cases} \underline{P_{k,is,j}} = \max\limits_{\forall i \in \mathbb{E}_j, j \in \mathbb{J}} P_k(i) \\ \text{s.t. } P_k(i) < 0 \quad \forall k \in \mathbb{K} \\ \quad S_c(i) = 0 \quad \forall c \in \mathbb{C} \end{cases} \tag{4e}$$

$$\begin{cases} \underline{P_{k,se,j}} = \min\limits_{\forall i \in \mathbb{E}_j, j \in \mathbb{J}} P_k(i) \\ \text{s.t. } P_k(i) < 0 \quad \forall k \in \mathbb{K} \\ \quad S_c(i) = 1 \quad \forall c \in \mathbb{C} \end{cases} \tag{4f}$$

The remaining symbols are the same as those in (1).

We can then provide the inter-corridor transfer constraints in an online dispatch, as shown in (5).

$$\underline{P_{k,j}} \le P_{k,j} \le \overline{P_{k,j}} \quad j \in \mathbb{E}_j, k \in \mathbb{K} \tag{5}$$

Constraint (5) intuitively shows that the proposed method transforms the old single limit in (3) into a finer transfer limit rule with $|\mathbb{J}|$ bands. Comparing the proposed model (4) with model (1), this idea permits a wider exploitation of security operations near the security boundary to maximize the use of inter-corridors.

III. Cluster and Classification Combined Online Banding Method for Power Transfer Limit

A. Cluster-based Offline Power Transfer-limit Banding

Operational data should be prepared prior to transfer-limit banding. This can be achieved by using good point-set sampling (GPS) over a parametric space and by collecting historical data. Specifically, we utilize existing operating limits to establish such a space, and the GPS is deployed in this space. Therefore, the input features are defined as: {active/reactive outputs of generators including synchronous generators and wind generators, active/reactive loads, terminal voltages, overall active loads}. Note that the on/off conditions of the generators are implicit in the power outputs (i.e., 0 denotes an off condition), and all inputs can be directly obtained. To simplify, the inputs are denoted by $\boldsymbol{x} \in \mathbb{R}^{n \times p}$ and outputs by $\boldsymbol{y} \in \mathbb{R}^{n \times \kappa}$. In addition, the overall transfer-limit decision task for all inter-corridors is separated into κ subtasks whose output is $\boldsymbol{y}_i$ ($i = 1, 2, \ldots, \kappa$), and in the subsequent description, $\boldsymbol{y}$ represents $\boldsymbol{y}_i$. Here, a subtask refers to the determination of the transfer limit for a specified inter-corridor. We deploy our method on each inter-corridor. Therewith, $\kappa = |\mathbb{K}|$.

Following the above idea, the UL was first introduced to produce several operating scenario clusters. The database for learning originates from historical operations and generates unseen unstable or extreme operating conditions (i.e., set $\mathbb{E}$), which are composed of critical operating variables formed as:

$$\boldsymbol{x} = \left[\boldsymbol{x}_1; \boldsymbol{x}_2; \ldots; \boldsymbol{x}_i; \ldots; \boldsymbol{x}_n\right] \quad \forall \boldsymbol{x}_i \in \mathbb{R}^{1 \times p}, \boldsymbol{x} \subseteq \mathbb{E} \tag{6a}$$

$$\boldsymbol{x}_i = \left[\boldsymbol{P}_g, \boldsymbol{Q}_g, \boldsymbol{P}_D, \boldsymbol{Q}_D, \boldsymbol{V}_g, \text{sum}\left(\boldsymbol{P}_D\right)\right] \quad \forall g \in \mathbb{G} \bigcap \mathbb{W}, D \in \mathbb{D} \tag{6b}$$

$$\boldsymbol{C} = \left[\boldsymbol{c}_1; \boldsymbol{c}_2; \ldots; \boldsymbol{c}_j; \ldots; \boldsymbol{c}_k\right] \quad \forall \boldsymbol{c}_j \in \mathbb{R}^{1 \times p}, \boldsymbol{c}_j \subset \boldsymbol{x}, k = |\mathbb{J}| \tag{6c}$$

The collected data were subjected to unsupervised learning. This paper uses the *K*-means++ algorithm to produce clusters to band-transfer limits, as *K*-means++ improves clustering accuracy and convergence compared with practical *K*-means. *K*-means++ executes the following process.

1) k centers $\mathcal{C} = \left[\boldsymbol{c}_{1,0}; \boldsymbol{c}_{2,0}; \ldots; \boldsymbol{c}_{k,0}\right]$ are arbitrarily initialized, where the second subscript denotes the number of iterations.

2) Starting from the i^{th} center, all data points closer to $\boldsymbol{c}_i$ than others $\boldsymbol{c}_j$ ($j \neq i$) are enfolded into the corresponding cluster.

3) For each cluster $i = 1, 2, \ldots, k$, the center is set as C_i: $\boldsymbol{c}_{i,1} = \dfrac{1}{|C_i|} \sum\limits_{\boldsymbol{x} \in C_i} \boldsymbol{x}$, where $|C_i|$ is the number of points in the cluster.

4) Iterations are counted, and 2) and 3) are repeated until C_i ($i = 1, 2, \ldots, k$) remains unchanged.

The proposed framework aims to identify the cluster to which an unseen operation belongs. Therefore, the clustering result is a target for real-time classifiers. For a given operating scenario, the cluster assignment is set as the classification label. We can obtain:

$$y = \left\{i | i = 1, 2, \ldots, k\right\} \tag{7}$$

Remark: in future, we will combine classification methods to enable real-time cluster attribution identification. Once the cluster to which an online operating condition belongs is determined, the transfer limit for the condition can be obtained by matching the associated transfer limit value of the cluster.

B. Identification of Critical Decision Variables

It is computationally inapplicable to involve all the parameters or variables in transfer-limit banding. Therefore, the critical variables must be identified. The mean impact value (MIV) method is used to determine barriers. The MIV first uses data to train neural networks (NNs). The responses of the NNs resulting from the perturbations of each input are then used as indices to determine the significance of the inputs. Therefore, a strong and robust NN structure is required. Thus, a multi-layer NN is used in this paper. As multi-label classifiers generally use *Softmax* layers to provide the probability of each label, which is a regression task, MIV method is available.

The mathematical model is given as:

$$\begin{cases} \boldsymbol{O}_1 = \mathcal{S}\left(\mathcal{M}_1(\boldsymbol{x})\right) \\ \boldsymbol{O}_2 = \mathcal{S}\left(\mathcal{M}_2\left(\boldsymbol{O}_1\right)\right) \\ \vdots \\ \boldsymbol{O}_{\mathcal{L}-1} = \mathcal{S}\left(\mathcal{M}_{\mathcal{L}-1}\left(\boldsymbol{O}_{\mathcal{L}-2}\right)\right) \\ \Phi^{\phi}(\boldsymbol{x}) = \mathcal{O}\left(\boldsymbol{O}_{\mathcal{L}-1}\right) \end{cases} \tag{8}$$

$$\boldsymbol{\phi}^* = \arg\min_{\theta} \left\| \boldsymbol{y} - \Phi^{\phi}(\boldsymbol{x}) \right\| + \lambda_n \left\| \boldsymbol{\phi} \right\|_2 \tag{9}$$

$$v_i^{MIV}=\text{mean}\left(\Phi^{\phi^*}\left([\boldsymbol{x}_1,\ldots,\boldsymbol{x}_a(1+\epsilon),\ldots,\boldsymbol{x}_p]\right)-\Phi^{\phi^*}\left([\boldsymbol{x}_1,\ldots,\boldsymbol{x}_a(1-\epsilon),\ldots,\boldsymbol{x}_p]\right)\right)\quad a=1,2,\ldots,p \tag{10}$$

where $\mathcal{M}$ and $\mathcal{S}$ are the affine function and activation function of the neural network, respectively; $\boldsymbol{O}_i$ is the output of the i^{th} hidden layer; Φ^{ϕ} is a compact representation for the NN; and ϕ stands for the parameters of the NN. In addition to the exogenous analysis of the MIV, the endogenous impacts of NN structures should also be considered. The hyperparameters of NNs contribute to the learning of in-depth patterns of outputs versus inputs. Therefore, we propose a feedforward method. For the multilayer NN structure provided in (8), the contributions from the i^{th} neuron in the l^{th} layer to the j^{th} neuron $(l+1)^{\text{th}}$ layer can be calculated using (11) and (12).

$$u_{l+1\leftarrow l}^{j-i}=\frac{\text{cov}\left(\mathcal{M}_{l+1}^{j}(\boldsymbol{O}_l),\boldsymbol{O}_l^i\right)}{\text{var}\left(\mathcal{M}_{l+1}^{j}(\boldsymbol{O}_l)\right)}\theta_{l+1\leftarrow l}^{j-i} \tag{11}$$

$$\boldsymbol{u}_{l+1\leftarrow l}=\left[u_{l+1\leftarrow l}^{j-i}\right]\in\mathbb{R}^{m_{l+1}\times m_l} \tag{12}$$

where the subscript indicates the two adjoining layers, and the superscript denotes the locations of specified neurons in the two layers. cov(·) and var(·) are the calculation functions of covariance and variance, respectively.

In the deployment feedforward process of (13), the influence of the i^{th} input on the output can be quantified.

$$v_i^{\text{Endo}}=\prod_{l=0}^{\mathcal{L}-1}\boldsymbol{u}_{l+1\leftarrow l}\quad \boldsymbol{O}_0=\boldsymbol{x}_{\cdot i} \tag{13}$$

By integrating (10) and (13), the importance of the i^{th} input is finally obtained using (14).

$$v_i=\frac{\left|v_i^{MIV}\odot v_i^{\text{Endo}}\right|}{Z}\quad i=1,2,\ldots,p \tag{14}$$

where $\odot$ denotes the elementwise multiplication.

By considering variables whose MIVs are above a given threshold, the critical variables that impact the transfer-limit banding are filtered. A compressed feature group can accurately and efficiently represent the operating patterns. Moreover, it is much easier to know the control variables to be regulated and the extent to which they must be. For simplification, we continue to use $\boldsymbol{x}$ to denote the compressed input features.

C. Classification-based Online Transfer-limit Decision

After identifying the critical decision variables, unseen operations are categorized into clusters, with only the principal features informed. Thus, the inputs for online transfer-limit decisions are prescribed as variables screened by the MIV, and the output is the cluster numbers. Each cluster corresponds to a single transfer-limit banding level. To ensure the conservativeness of the banding, we determine the banding level according to (15).

$$m=\arg\max_{1,2,\ldots,k}\Phi^{\phi^*}(\boldsymbol{x}) \tag{15a}$$

$$\Gamma_{ij,s}=P_{s,m}\quad \forall s\in\mathbb{K} \tag{15b}$$

Here $\Gamma_{ij,s}$ is introduced to simplify the later model illustration, and it is the same as the above transfer limit symbol in (1), (3), (4), and (5). $\Phi^{\phi^*}(\boldsymbol{x})$ is the trained classifier and calculates probabilities that operation $\boldsymbol{x}$ may locate in a cluster. Using the argmax operator, (15a) finally determines to which cluster $\boldsymbol{x}$ pertains. Here, m is a cluster. Subsequently, (15b) assigns the corresponding transfer limit to $\boldsymbol{x}$. For a better understanding, the traditional method and proposed method of calculating the online transfer limit are visualized in Fig. 3. The traditional method conducts the most conservative transfer capability corresponding to the most conservative extreme operating scenario to steer online dispatch, such that all operations run beyond the limit are discarded. Instead, the proposed method determines transfer limits for each typical cluster of operations. An extra transfer limit profile is introduced for Cluster 1. In this regard, the operations that are discarded in traditional implementation are reused, which are located between the two dot-dashed lines.

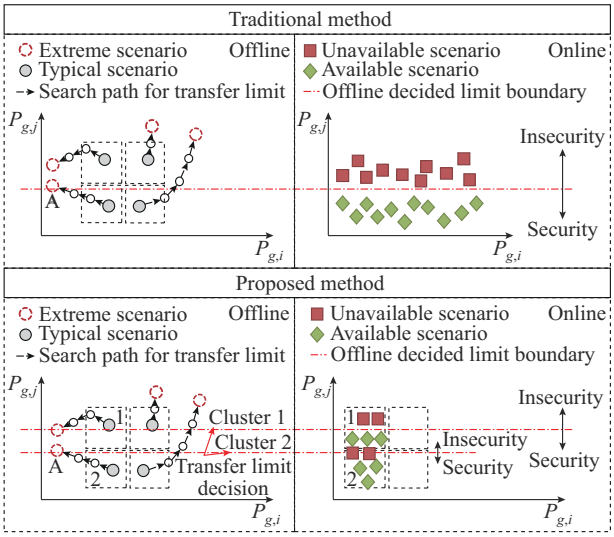

Fig. 3. Comparative diagram of traditional method and proposed method.

Figure 3 shows that the traditional method applies the most conservative transfer limit, such that there are numerous unnecessary scenario discards. More than half of the scenarios are set as unavailable, but not all of these unavailable scenarios are insecure. The proposed method establishes finer transfer-limit rules for reusing these scenarios. Instead of setting a bottom limit for all the operations, the proposed method provides a limit for each typical operating cluster. This benefits the original unavailable scenarios being reactivated such that the availability of inter-corridors is improved.

Equations (4) and (15) indicate that the minimum power flow over an unstable operating cluster is the transfer capability in this scenario. This is supported by the important evidence that there exists a practical hyperpolyhedron-sketched dynamic security region composed of prefault power generation coordinates. In other words, the endogenous stability boundary of a specified power system enables us to approximate the local security boundary for each operating cluster. In this analysis, to implement (4) and (15), the stability conditions must be known and collected during data preparation in Section III-A.

Several methods have been developed to achieve this goal. Because data are prepared offline, which means that efficiency is not demanding, precision is valued more than speed at this stage. Therefore, we conduct a time-domain simulation (TDS) to infer the transient stability. TDS applies numerical computation to capture the trajectories of DAEs instead of finding an analytical solution [16]. This fits well with solving large-scale and high-order DAEs, and is thus compatible with precise transient stability analysis.

In practice, a critical demand is that the decision must be sufficiently conservative to ensure secure operation. This is also the pivot point that a classifier for transfer-limit banding should follow. Therefore, we introduce a cost-sensitive learning technique. The cost-sensitive learning in [17] is adopted. The cost-sensitive matrix is predefined following a conservative prior; that is, if the trained learner is blurred to determine the transfer limit among several bands, the priority will be to set the minimal limit. This also refers to the concept of false-negative risk prevention, as it is known that errors in online classification always exist, even if the performance of the classifiers has been augmented offline to the utmost extent. In this premise, we preset the learning bias as:

$$\varpi_{ij}=P_{k,j}/P_{k,i} \tag{16a}$$

$$Y_{ij}=\begin{cases}1 & \varpi_{ij}\le 1\\ 1+10\lg\varpi_{ij} & \text{else}\end{cases} \tag{16b}$$

$$\begin{bmatrix}1 & Y_{12} & \cdots & Y_{1|\mathbb{J}|}\\ Y_{21} & Y_{22} & \cdots & Y_{2|\mathbb{J}|}\\ \vdots & \vdots & & \vdots\\ Y_{|\mathbb{J}|1} & Y_{|\mathbb{J}|2} & \cdots & 1\end{bmatrix} \tag{16c}$$

where the columns and rows correspond to the predicted and true labels, respectively. Equations (16a) and (16b) indicate that if the predicted transfer limit is larger than the true value, a significant penalty will be weighed on the training loss; otherwise, the loss will be maintained. This strategy allows the classifier to make conservative decisions and reduces the risk of false negatives. Finally, the matrix (16c) directly affects the learning loss.

To highlight the essence of this paper, details of the cost-sensitive learning process are ignored.

D. An Optimization-based Showcase for Cluster and Classification Combined Banding Rules

It is expected that the over-conservativeness issue is fixed to some extent because a finer transfer-limit banding rule activates more security operating modes that are discarded in the previous single-transfer limit. The next step is to flexibly tune the operation such that the transfer potential of the critical inter-corridors can be used. Classification-based decisions provide a straightforward and fast way to determine how the transfer limit varies with operations as well as control information, but no nonlinear operation is required. This is useful for dispatching tasks. In this paper, we instantiate an optimization-based showcase to justify the entire workflow.

An economic dispatch model is then devised, where the intention is to optimize power system operations under strict power transfer security constraints. This model is given by (17).

$$\begin{cases}\min\sum_{t=k+1}^{k+u}\Delta t\left(\sum_{g\in\mathbb{G}}C_g\left(P_g(t)\right)+\sum_{w\in\mathbb{W}}C_w\left(\Delta P_w(t)\right)\right)\\ C_g\left(P_g\right)=a_gP_g^2+b_gP_g+c_g\\ C_w\left(\Delta P_w\right)=c_w\Delta P_w\\ \text{s.t. } P_g^{\min}<P_g(t)<P_g^{\max}\\ \quad \Delta P_g^{\min}<P_g(t+1)-P_g(t)<\Delta P_g^{\max}\\ \quad Q_g^{\min}<Q_g(t)<Q_g^{\max}\\ \quad P_i^{Inj}(t)-V_i(t)\sum_{j\in i}V_j(t)\left(G_{ij}\cos(\theta_{ij,t})+B_{ij}\sin(\theta_{ij,t})\right)=0\\ \quad Q_i^{Inj}(t)-V_i(t)\sum_{j\in i}V_j(t)\left(G_{ij}\sin(\theta_{ij,t})-B_{ij}\cos(\theta_{ij,t})\right)=0\\ \quad P_i^{Inj}(t)=P_i^{Gen}(t)-P_i^{Load}(t)\\ \quad Q_i^{Inj}(t)=Q_i^{Gen}(t)-Q_i^{Load}(t)\\ \quad V_i^{\min}(t)<V_i(t)<V_i^{\max}(t)\\ \quad P_{ij,l}^{\min}(t)<P_{ij,l}(t)<P_{ij,l}^{\max}(t)\\ \quad 0\le\Delta P_w(t)\le P_w^{Fore}(t)\\ \quad P_w^{Fore}(t)=\begin{cases}P_w^{Fore}(t) & 0\le P_w^{Fore}(t)<P_w^{\max}(t)\\ P_w^{\max}(t) & P_w^{Fore}(t)\ge P_w^{\max}(t)\end{cases}\\ \quad P_w(t)=P_w^{Fore}(t)-\Delta P_w(t)\\ \quad P_w^{\min}(t)\le P_w(t)\le P_w^{\max}(t)\end{cases} \tag{17a}$$

$$\eta_s(t)\triangleq P_{ij,s}(t)-\Gamma_{ij,s}(t)\le-\epsilon \tag{17b}$$

$$\forall g\in\mathbb{G},k\in\mathbb{T},i,j\in\mathbb{B},l\in\mathbb{L},w\in\mathbb{W},s\in\mathbb{K} \tag{17c}$$

In (17b), $\Gamma_{ij,s}(t)$ is also a variable which is decided by operations. Back to Sections III-A and III-B, we know that once the cluster to which current operation belongs is found, $\Gamma_{ij,s}(t)$ can be identified via (4) and (15).

Because this paper demonstrates the effectiveness of enhancing the utilization of power inter-corridors via the proposed data-driven banding method for power transfer limit, we do not focus on a detailed optimization algorithm design. Here, a distributed genetic algorithm (DGA) is proposed to solve model (17). Using simplified model (17) as (18), the DGA-solving model can be denoted as (19).

$$\begin{cases}\min f(\boldsymbol{x})\\ \text{s.t. } h(\boldsymbol{x})=0\\ \quad g(\boldsymbol{x})\le 0\end{cases} \tag{18}$$

$$P(\boldsymbol{x})=f(\boldsymbol{x})+\mu_1h(\boldsymbol{x})+\mu_2\rho\left(g(\boldsymbol{x})\right) \tag{19a}$$

$$\boldsymbol{\rho}(\boldsymbol{y})=\begin{cases}\boldsymbol{0} & \boldsymbol{y}\le\boldsymbol{0}\\ \boldsymbol{y} & \boldsymbol{y}>\boldsymbol{0}\end{cases} \tag{19b}$$

where $f(\boldsymbol{x})$, $h(\boldsymbol{x})$, and $g(\boldsymbol{x})$ are the compact forms of the objective, equality, and inequality constraints in (18); $P(\boldsymbol{x})$

is the transformed optimization objective with penalties. $\boldsymbol{\rho}(\boldsymbol{y})$ is a function of accumulating inequality constraint violations, i.e., for the constraints $g(\boldsymbol{x})\leq 0$, the portion that exceeds 0 is included in penalty function $P(\boldsymbol{x})$.

The implementation process of the proposed method is illustrated in Fig. 4. We take a new *K*-means++ based transfer limit decision scheme at the offline stage, for uncovering more available power transfer potential of inter-corridors. The *K*-means++ naturally provides a controllable transfer limit set by introducing its cluster affiliation conditions, which will be further accelerated and reduced by cost sensitive learning. At the online stage, this controllable transfer limit set is seamlessly incorporated with economic dispatch to realize the utilization optimization for inter-corridors.

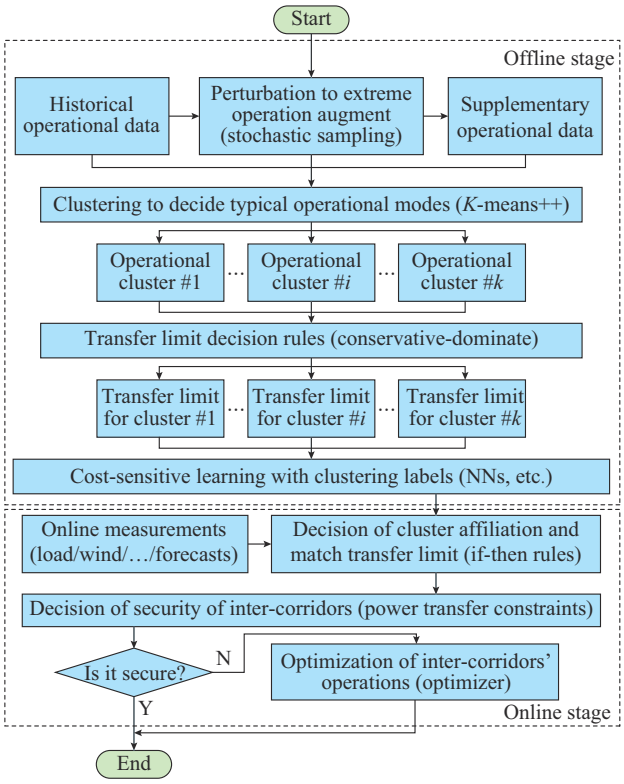

Fig. 4. Implementation process of proposed method.

IV. Numerical Results

A. Test Systems and Generation of Data Samples

The proposed method is tested using a modified IEEE 39-bus system [18]. A wind farm with a rated power output of 500 MW is set on Bus 17. For the settings of the transient stability verification and TDS, the fault type is set as three-phase short-circuit fault of the critical power transfer inter-corridors. For a given operating condition, contingency involves the set faults on intact grid and the grid with $N-1$ occurrence. The sampling space for the generation of generators and active loads is the nominal output range and 80%-120% of the baselines. As for the generators' terminal voltages, 0.95-1.05 p.u. is selected. The reactive loads vary with the active loads to maintain their corresponding constant power factors. Following the above sampling procedure, 16000 samples constitute the training set, 2000 samples are used as the validation set, and 10350 samples are used as the test dataset. Each sample is composed of a 63-dimension input vector and a cluster affiliation label.

B. Cluster-based Banding Method for Power Transfer Limit

To visualize the banding process for power transfer limit, we provided five different scenarios, including deciding the transfer limit via the most conservative criterion and banding limit by 3, 5, 10, and 20 levels, respectively. The results are shown in Fig. 5, where different colors and types of marks denote features from distinct clusters.

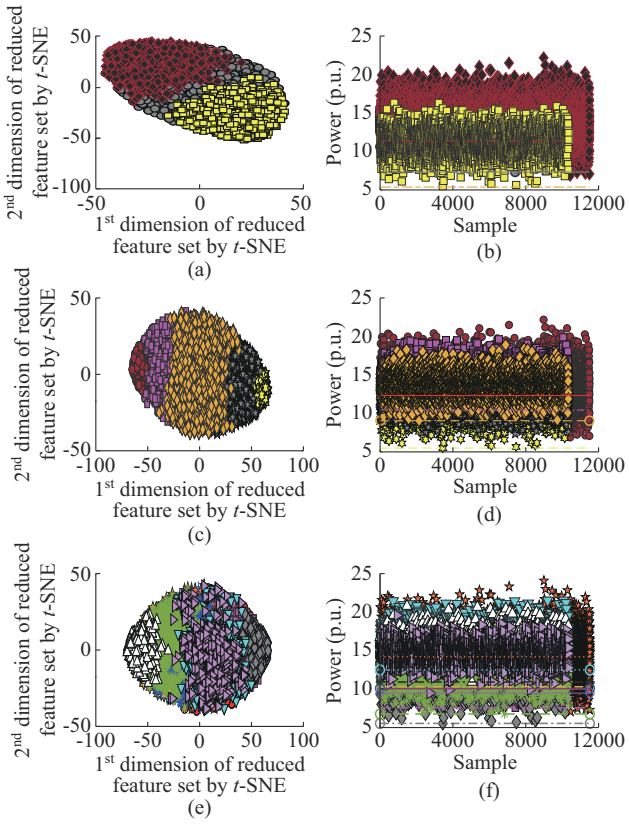

Fig. 5. Outcomes of proposed cluster-based banding method. (a) 3-cluster banding. (b) Transfer-limit decision with 3 bands. (c) 5-cluster banding. (d) Transfer-limit decision with 5 bands. (e) 10-cluster banding. (f) Transfer-limit decision with 10 bands.

As shown in Fig. 5, because numerous features are involved in clustering, it is impossible to directly visualize the clustering outcomes in a 2-dimension space. Thus, we introduced *t*-distributed stochastic neighbor embedding (*t*-SNE) to embed the original 63 dimensions into a 2-dimension space [19]. Figures 5(a), (c), and (e) are obtained using the *t*-SNE. It can be observed that, along with an increasing number of clusters, a finer typical scenario partition is enabled. This is a notable conclusion; however, it induces an interesting byproduct. Figures 5(b), (d), and (e) show that higher maximal transfer limits result in finer clustering. In detail, the maximal transfer limits for 3, 5, and 10 clusters are 13.59 p.u., 14.35 p.u., and 15.22 p.u., respectively. For non-

clustering and 20 clusters scenarios, they are 12.62 p.u. and 16.30 p. u., respectively. From this data, we can conclude that more clusters can positively impact the utilization level for inter-corridors. Theoretically, the ideal case involves associating each operating condition with a transfer limit. This roadmap has been previously outlined in [18]. However, we find that because the precise transfer-limit computation model is overly complicated and has strong nonlinearity, such that the time consumption of offline data preparation is too costly, it is too difficult to practically implement one-to-one transfer-limit decisions for each operation. Fortunately, the proposed method can be considered as a compromise between traditional over-conservative decisions and ideal methods. In the proposed method, although more clusters can promote greater utilization of inter-corridor power transfer, an increased scale of the learning dataset is required. Therefore, careful consideration of the tradeoff between learning and operating efficiency is necessary. We find that a range of 10-20 clusters is sufficient to securely improve the utilization of inter-corridors; however, it is not a theoretically optimal choice. As this issue is not the major focus of this paper, we will attempt to address it in the future.

Table I and Fig. 6 provide transfer-limit banding outcomes and stacked bar chart of transfer-limit banding level under different clustering conditions. We will follow these banding to further improve operations.

TABLE I
TRANSFER LIMIT BANDING OUTCOMES UNDER DIFFERENT CLUSTERING CONDITIONS

Clustering condition	Transfer-limit banding (from low to high) (p.u.)
Conservative	12.62
3-cluster	12.62, 12.94, 13.60
5-cluster	12.62, 12.94, ..., 14.35
10-cluster	12.62, 12.94, ..., 15.22
20-cluster	12.62, 12.94, ..., 16.30

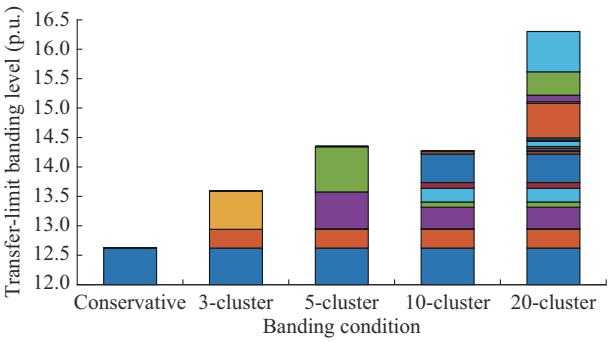

Fig. 6. Stacked bar chart of transfer-limit banding level under different clustering conditions.

As listed in Table I and Fig. 6, a finer transfer-limit banding results in greater utilization of the power transfer inter-corridors. Compared with the most conservative scheme, the maximal transfer limit of the finest strategy is improved by 29.16%.

C. Cost-sensitive Classifier-based Online Transfer-limit Decision

In the online dispatch stage, straightforward rules are preferred to tune the power transfers for more efficient and economical operations. In this subsection, we do not care about the structure of such rules, but intend to provide cautious decision-making to ensure that power transfer operates securely. Cost-sensitive neural networks (CSNNs) are adopted. To illustrate the conservativeness via the CSNN, we provide the confusion matrix outcomes tested on the testing dataset, as shown in Tables II-V. Additionally, comparative studies are conducted using non-cost-sensitive NNs, as given in Tables II and IV.

TABLE II
CONFUSION MATRIX OF TRANSFER-LIMIT DECISION WITH 3 BANDS BY NON-COST-SENSITIVE NNS

Transfer-limit banding level	Prediction, 1/12.62 p.u.	Prediction, 2/13.60 p.u.	Prediction, 3/12.94 p.u.
True label, 1/12.62 p.u.	2885	0	24
True label, 2/13.60 p.u.	0	2783	15
True label, 3/12.94 p.u.	17	18	4608

TABLE III
CONFUSION MATRIX OF TRANSFER-LIMIT DECISION WITH 3 BANDS BY CSNNS

Transfer-limit banding level	Prediction, 1/12.62 p.u.	Prediction, 2/13.60 p.u.	Prediction, 3/12.94 p.u.
True label, 1/12.62 p.u.	2909	0	0
True label, 2/13.60 p.u.	0	2706	92
True label, 3/12.94 p.u.	90	0	4553

TABLE IV
CONFUSION MATRIX OF TRANSFER-LIMIT DECISION WITH 5 BANDS BY NON-COST-SENSITIVE NNS

Transfer-limit banding level	Prediction, 1/12.95 p.u.	Prediction, 2/13.58 p.u.	Prediction, 3/12.94 p.u.	Prediction, 4/12.62 p.u.	Prediction, 5/14.35 p.u.
True label, 1/12.95 p.u.	2973	11	13	0	0
True label, 2/13.58 p.u.	10	2431	0	0	4
True label, 3/12.94 p.u.	10	0	2482	14	0
True label, 4/12.62 p.u.	0	0	18	1235	0
True label, 5/14.35 p.u.	0	8	0	0	1141

Recall the conservativeness demand mentioned in Section III-C, i.e., which strictly prohibits the classifier from overestimating the true transfer limit. We begin the analysis by comparing the data in Tables II and III. To clarify the improvements of the CSNN, we highlight the concerned elements of confusion matrices, which can explain how the CSNN addresses conservativeness. In Tables II-V, the nota-

tion "1/12.62 p.u." denotes that the transfer-limit banding level at the first band is set to be 12.62 p.u.. In the unseen data testing, there are 24 scenarios that the non-cost-sensitive classifier overestimates the transfer-limit banding of 12.62 p.u. (label 1) to that of 12.94 p.u. (label 3), and the same case also happens 18 times on judging between the transfer limits of 12.94 p.u. (label 3) and 13.60 p.u. (label 2). These misclassifications are not allowed in online decision-making because the actual power transfer may exceed the limit, and further security risk can be induced. Fortunately, such risks can be circumvented through CSNNs. This argument is presented in Table III, and the number of overestimated cases is reduced to 0. Extending this to other situations, the same observations can be made, as shown in Tables IV and V.

TABLE V
CONFUSION MATRIX OF TRANSFER-LIMIT DECISION WITH 5 BANDS BY CSNNS

Transfer-limit banding level	Prediction, 1/ 12.95 p.u.	Prediction, 2/ 13.58 p.u.	Prediction, 3/ 12.94 p.u.	Prediction, 4/ 12.62 p.u.	Prediction, 5/ 14.35 p.u.
True label, 1/12.95 p.u.	2940	1	56	0	0
True label, 2/13.58 p.u.	33	2411	0	0	1
True label, 3/12.94 p.u.	0	0	2456	50	0
True label, 4/12.62 p.u.	0	0	1	1252	0
True label, 5/14.35 p.u.	0	39	0	0	1110

Moreover, misclassifications are transferred to the conservative cases. This result is due to the fact that cost-sensitive classifiers are more likely to identify a true transfer limit to a lower value. For instance, as for the 5-band classifiers, a conservative identification of transfer limit is to decide true transfer limit of 13.58 p.u. (label 2) to 12.95 p.u. (label 1). The corresponding data in the confusion matrices are shown in Tables IV and V. Evidently, the CSNN results in more frequencies of 33 than 10 when using non-cost-sensitive NNs. In other words, CSNN enables conservative decision-making for the transfer limit.

Combined with the conclusions presented in Section IV-B, a worthy concern emerges: how does the performance of the classifier vary with finer transfer-limit banding and more banding levels? Thus, the online transfer-limit decision precision trends along with the number of bands are given in Fig. 7.

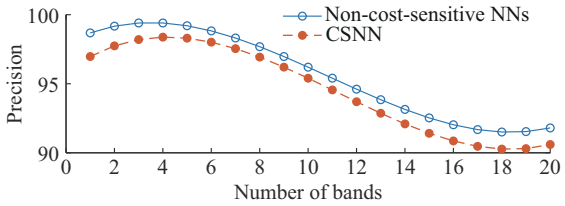

Fig. 7. Online transfer-limit decision precision trends along with number of bands.

As shown in Fig. 7, there is a clear trend of decreasing precision as the banding becomes finer. The precision is reduced to approximately 90% at the finest banding condition of 20-cluster. However, it should be noted that our prepared sample size is fixed, such that finer banding would result in fewer samples for each label. Therefore, the tendency shown in Fig. 7 is unsurprising. Following this analysis, a larger dataset could address this issue. Fortunately, this can be easily achieved using operating simulations, stochastic sampling, and engineering software.

In addition, the transfer-limit decision elapsed time of the well-built classifiers is less than 1 s on average. This supports the online application of the transfer-limit banding rule.

D. Economic Dispatch Showcase

To justify the proposed transfer-limit banding rules for online dispatch, the outcomes of a showcase are presented. We report 5 transfer-limit banding conditions to highlight superiority of our method, i.e., rule 1 (the most conservative rule), rule 2 (transfer-limit rule with 3 bands), rule 3 (transfer-limit rule with 5 bands), rule 4 (transfer-limit rule with 10 bands), and rule 5 (transfer-limit rule with 20 bands). A 24-hour economic dispatch instance with a timescale of 1 hour is designed and tested. Figure 8 presents the operating conditions of the inter-corridors before and after economic dispatch, and the outcomes of rules 1-5 are sequentially presented from top to bottom. The subplots on the left show the operations before dispatch, whereas the subplots on the right show the dispatch results.

It can be observed from the data in Fig. 8 that, dispatch guided by rule 1 cannot find a feasible solution that constrains power transfer. Specifically, the power flow still exceeds the transfer limit during the 13-16 hours. These results are based on the fact that the over-conservativeness premise cuts the operating region excessively. In practice, such security violations are usually nonexistent because an adequate security margin is reserved for the power infrastructure. However, resource wastage is widespread. Considering the finer transfer limit rule, it can be observed that all dynamic rules (i.e., rules 2-5) fulfill the security constraints for power transfer inter-corridors, and the finer banding rules induce higher power transfers.

To demonstrate the positive influence of the finer transfer limit rule on wind power consumption, the wind curtailment profiles incurred by the testing rules are presented in Fig. 9. The wind curtailment results corresponding to rules 1-5 are listed in top-to-bottom order.

The results, as shown in Fig. 9, indicate that the proposed transfer-limit decision method enables the release of the power transfer potential. It can be observed that along with the finer transfer-limit banding rule, the wind curtailment steadily declines. According to rule 4, almost no abandoned wind power exists. The argument again underlines that the traditional over-conservative transfer-limit decision method significantly confines the utilization of inter-corridors and renewable energy consumption.

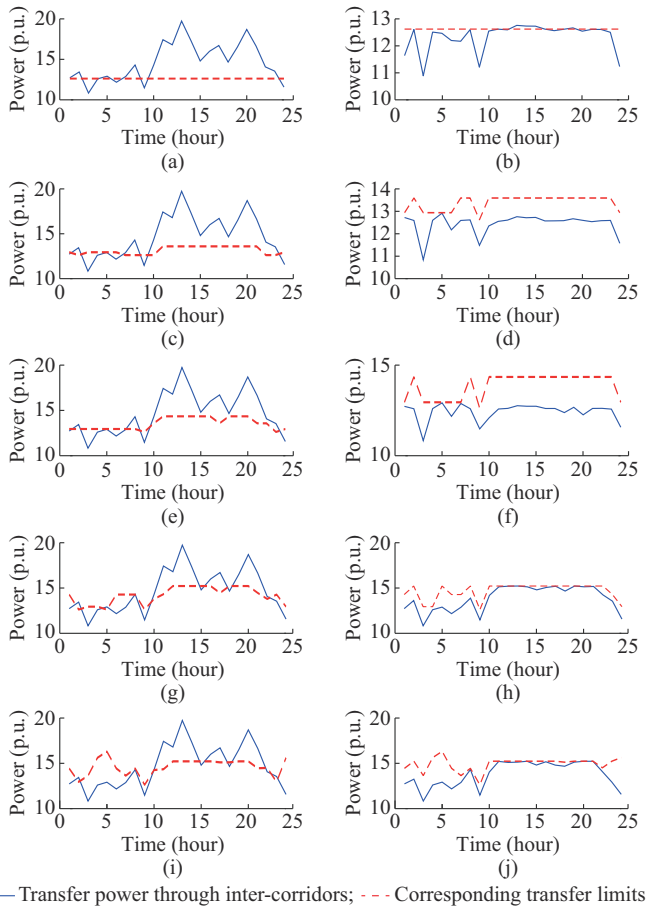

Fig. 8. Operating conditions of inter-corridors before and after economic dispatch. (a) Power using rule 1 before economic dispatch. (b) Power using rule 1 after economic dispatch. (c) Power using rule 2 before economic dispatch. (d) Power using rule 2 after economic dispatch. (e) Power using rule 3 before economic dispatch. (f) Power using rule 3 after economic dispatch. (g) Power using rule 4 before economic dispatch. (h) Power using rule 4 after economic dispatch. (i) Power using rule 5 before economic dispatch. (j) Power using rule 5 after economic dispatch.

E. Numerical Study on a Real-world Power System in China

The proposed method is verified using a real-world power system in China. The applied regional power system is located in Northwest China and comprises five provincial grids (Gansu, Shaanxi, Qinghai, Ningxia, and Xinjiang). The northwestern power system of China has over 7500 dispatchable generators including thermal units, hydropower units, wind power generators, and photovoltaic plants. There are more than 4000 transmission lines in the transmission-level system, of which four critical power transfer inter-corridors that affect system security are selected for the numerical study. The abbreviations used are GN, GX, GQ, and GS. $N-1$ and short-circuit faults on the critical inter-corridors as well as a few severe faults set from the dispatcher experience, are considered in the contingency.

We test the proposed method under two operating conditions, i.e., OC1 and OC2:

1) OC1: with a total load of 1.048391×10^5 MW and total renewable power generation of 3.42072×10^4 MW.

2) OC2: with a total load of 1.016834×10^5 MW and a total renewable power generation of 3.78922×10^4 MW.

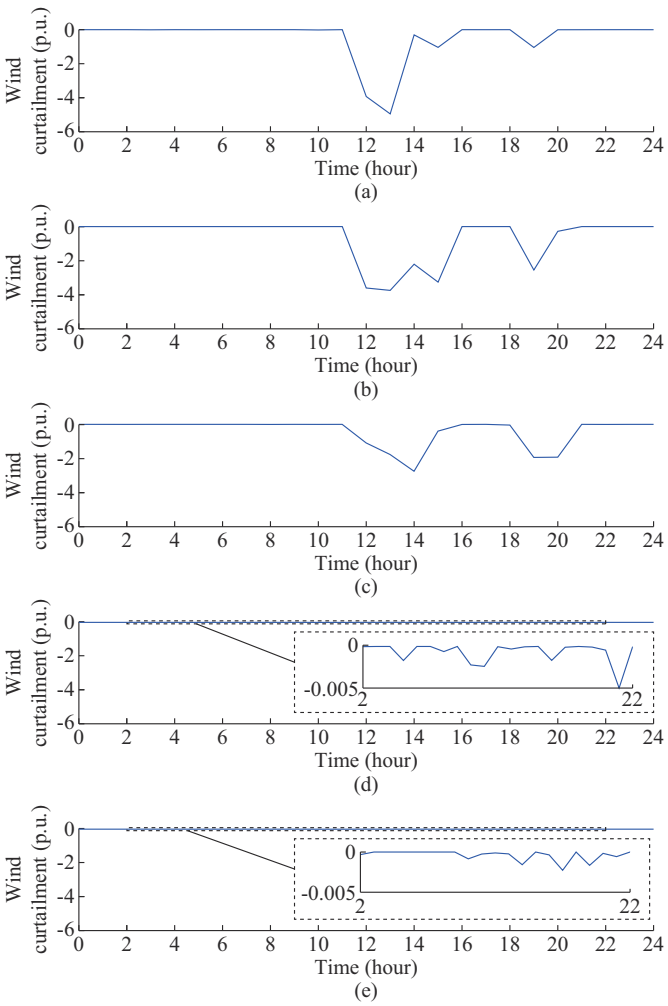

Fig. 9. Wind curtailment profiles incurred by testing rules. (a) Rule 1. (b) Rule 2. (c) Rule 3. (d) Rule 4. (e) Rule 5.

The outcomes of tuning transfer limits by the proposed method under OC1 and OC2 are listed in Tables VI and VII, respectively. The nominal power is 100 MW.

TABLE VI
OUTCOMES OF TUNING TRANSFER LIMITS BY PROPOSED METHOD UNDER OC1 (P.U.)

Inter-corridor	Power flow before tuning	Transfer limit before tuning	Power flow after tuning	Transfer limit after tuning	Transfer limit increase on average (%)
GN	67.45	56.98	64.02	65.27	10.42
GX	–29.86	–20.48	–20.21	–21.50	
GQ	–13.07	–2.21	–6.37	–6.44	
GS	49.94	34.94	31.79	33.65	

As observed from Tables VI and VII, an increase of over 10% in the transfer limit was realized using the proposed method, which demonstrates that the proposed method improves the usage of critical power transfer inter-corridors with strictly bounded operating security.

To further compare the proposed method with the traditional dispatch-experience-based method, we provide the testing outcomes of the GX, as shown in Fig. 10, where differ-

ent colors represent the transfer limits corresponding to different clusters.

TABLE VII
OUTCOMES OF TUNING TRANSFER LIMITS BY PROPOSED METHOD UNDER OC2 (P.U.)

Inter-corridor	Power flow before tuning	Transfer limit before tuning	Power flow after tuning	Transfer limit after tuning	Transfer limit increase on average (%)
GN	30.03	21.40	22.98	24.97	20.40
GX	–29.84	–14.88	–14.62	–15.35	
GQ	–18.09	–7.63	–8.04	–19.38	
GS	49.98	34.97	34.52	35.26	

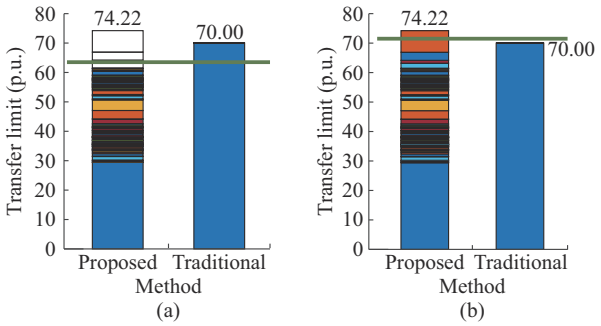

Fig. 10. Comparative outcomes of GX by proposed method and traditional method. (a) Before tuning. (b) After tuning.

In Fig. 10, the amount of power transferred is indicated by the green line. The empirical transfer limit of GX is determined to be 70 p.u.. This transfer limit is the ground truth in the operation of the northwestern power system of China. Meanwhile, our method renders 74 transfer limit bands, and the highest value reaches 74.22 p. u.. The operating conditions of the GX before and after the power flow tuning are shown in the two subplots, respectively. According to Fig. 10, an empirical transfer limit of 70 p.u. restricts the ability of GX to transfer power prior to tuning. After deploying our method, the power transfer increases beyond the empirical limit, but it is still constrained by the fine transfer-limit banding. Therefore, the proposed method releases the potential of the power transfer inter-corridor while maintaining security. These analyses confirm the effectiveness of the proposed method.

V. CONCLUSION

In this paper, a new pragmatic data-driven method that enables fine and conservative transfer-limit control is proposed. The key is to use unsupervised cluster learning to identify typical operating patterns and determine the band-conservativeness-dominated transfer limit for each cluster. Subsequently, a cost-sensitive classifier is used to produce a fast and reliable rule for flexibly controlling the transfer limit. Finally, an optimization-based showcase is provided to justify the proposed method. The numerical results on the modified IEEE benchmark and a real-world power system in China show that compared with the current research, the proposed method enables a more practical implementation in engineering, as no intricate transfer-limit modeling is needed. However, in comparison with the traditional empirical method, the proposed method renders better utilization of power transfer inter-corridors while guaranteeing security. In future work, a faster deep-learning-aided sensitivity-based method will be studied to enhance transfer limit control with respect to efficiency and engineering practicability.

REFERENCES

[1] J. Zhao, M. Netto, Z. Huang *et al.*, "Roles of dynamic state estimation in power system modeling, monitoring and operation," *IEEE Transactions on Power Systems*, vol. 36, no. 3, pp. 2462-2472, May 2021.
[2] I. Dobson, S. Greene, R. Rajaraman *et al.* (2001, Jan.). Electric power transfer capability: concepts, applications, sensitivity and uncertainty. [Online]. Available: https://www. researchgate. net/publication/246040923_Electric_power_transfer_capability_concepts_applications_sensitivity_and_uncertainty
[3] A. L. Bettiol, L. Wehenkel, and M. Pavella, "Transient stability-constrained maximum allowable transfer," *IEEE Transactions on Power Systems*, vol. 14, no. 2, pp. 654-659, May 1999.
[4] M. Zhao, F. Li, X. Yao *et al.*, "Research on transient stability constrained total transfer capability calculation of large interconnected power system," in *Proceedings of 2010 International Conference on Power System Technology*, Hangzhou, China, Oct. 2010, pp. 1-6.
[5] L. Min and A. Abur, "Total transfer capability computation for multi-area power systems," *IEEE Transactions on Power Systems*, vol. 21, no. 3, pp. 1141-1147, Aug. 2006.
[6] A. L. da Silva, J. G. de Carvalho Costa, L. A. da Fonseca Manso *et al.*, "Transmission capacity: availability, maximum transfer and reliability," *IEEE Transactions on Power Systems*, vol. 17, no. 3, pp. 843-849, Aug. 2002.
[7] T. B. Nguyen and M. A. Pai, "Dynamic security-constrained rescheduling of power systems using trajectory sensitivities," *IEEE Transactions on Power Systems*, vol. 18, no. 2, pp. 848-854, May 2003.
[8] L. Tang and W. Sun, "An automated transient stability constrained optimal power flow based on trajectory sensitivity analysis," *IEEE Transactions on Power Systems*, vol. 32, no. 1, pp. 590-599, Jan. 2017.
[9] Q. Jiang and G. Geng, "A reduced-space interior point method for transient stability constrained optimal power flow," *IEEE Transactions on Power Systems*, vol. 25, no. 3, pp. 1232-1240, Aug. 2010.
[10] X. Zhang, Y. H. Song, Q. Lu *et al.*, "Dynamic available transfer capability (ATC) evaluation by dynamic constrained optimization," *IEEE Transactions on Power Systems*, vol. 19, no. 2, pp. 1240-1242, May 2004.
[11] G. Geng, Q. Jiang, and Y. Sun, "Parallel transient stability-constrained optimal power flow using GPU as coprocessor," *IEEE Transactions on Smart Grid*, vol. 8, no. 3, pp. 1436-1445, May 2016.
[12] G. Qiu, Y. Liu, J. Liu *et al.*, "Surrogate-assisted optimal re-dispatch control for risk-aware regulation of dynamic total transfer capability," *IET Generation, Transmission & Distribution*, vol. 15, no. 13, pp. 1949-1961, May 2021.
[13] Y. Liu, J. Zhao, L. Xu *et al.*, "Online TTC estimation using nonparametric analytics considering wind power integration," *IEEE Transactions on Power Systems*, vol. 34, no. 1, pp. 494-505, Jun. 2018.
[14] Q. Hou, E. Du, N. Zhang *et al.*, "Impact of high renewable penetration on the power system operation mode: a data-driven approach," *IEEE Transactions on Power Systems*, vol. 35, no. 1, pp. 731-741, Jan. 2019.
[15] M. Ramezani, C. Singh, and M.-R. Haghifam, "Role of clustering in the probabilistic evaluation of TTC in power systems including wind power generation," *IEEE Transactions on Power Systems*, vol. 24, no. 2, pp. 849-858, May 2009.
[16] Y. Liu, K. Sun, R. Yao *et al.*, "Power system time domain simulation using a differential transformation method," *IEEE Transactions on Power Systems*, vol. 34, no. 5, pp. 3739-3748, Nov. 2019.
[17] M. Kukar and I. Kononenko, "Cost-sensitive learning with neural networks," *ECAI*, vol. 15, no. 27, pp. 88-94, Jun. 1998.
[18] G. Qiu, Y. Liu, J. Zhao *et al.*, "Analytic deep learning-based surrogate model for operational planning with dynamic TTC constraints," *IEEE Transactions on Power Systems*, vol. 36, no. 4, pp. 3507-3519, Jul. 2020.
[19] L. van der Maaten and G. Hinton, "Visualizing data using *t*-SNE," *Journal of Machine Learning Research*, vol. 9, no. 11, pp. 2579-2605, Nov. 2008.

Lidong Yi received the B.S., M.S., and Ph.D. degrees in School of Electrical Engineering from Xi'an Jiaotong University, Xi'an, China, in 1988, 1991, and 1995, respectively. He was a Senior Engineer with State Grid Ningxia Electric Power Co.. Ltd., Yinchuan, China, and is currently the Chairman of State Grid Sichuan Electric Power Company, Chengdu, China. His research interests include transmission power system operation and planning, power system security, power system stability, insulation technology, high-voltage power transmission, and new energy.

Maosheng Ding received the Ph. D. degree in electrical engineering from South China University of Technology, Guangzhou, China, in 2005. He is now a Senior Engineer with the State Grid Ningxia Electric Power Company, Yinchuan, China. His research interests primarily include power system operation and control, renewable integration, and energy internet.

Jili Wang received the Ph.D. degree from North China Electric Power University, Beijing, China, in 2010. He is currently a Senior Engineer with the Northwest Branch, State Grid, Corporation of China, Xi'an, China. His research interests include power system stability and control, power system operational planning, renewable integration, and data-driven power system analysis.

Gao Qiu received the B.S. and Ph.D. degrees in electrical engineering from Sichuan University, Chengdu, China, in 2016 and 2021, respectively. He is now an Associate Research Fellow with the College of Electrical Engineering, Sichuan University. His current research interests include power system knowledge discovery and operation, artificial intelligence application in power system, power system stability and control, and dynamic transfer limit control.

Fei Xue received the M.S. degree in School of Electrical and Information Engineering from Tianjin University, Tianjin, China, in 2016. He is now an Engineer with the State Grid Ningxia Electric Power Company, Yinchuan, China. His current research interests include artificial intelligence application in power system, power system stability, and renewable energy modelling.

Ji'ang Liu received the M.S. degree in electrical engineering from Sichuan University, Chengdu, China, in 2022. He is now pursuing the Ph.D. degree in the College of Electrical Engineering, Sichuan University. His current research interests include power system knowledge discovery and operation, and artificial intelligence application in power system.

Yuxiong Huang received the B.S. and Ph.D. degrees in electrical engineering from Xi'an Jiaotong University, Xi'an, China, in 2017 and 2022, respectively. His main research interests include reliability evaluation and machine learning technologies in power systems.

Gengfeng Li received the Ph. D. degree in electrical engineering from Xi'an Jiaotong University, Xi'an, China, in 2014. He is currently a Professor with the School of Electrical Engineering, Xi'an Jiaotong University. His research interests include power system reliability evaluation, grid resilience, machine learning technologies in power systems, and integration of renewable energy.

Junyong Liu received the Ph.D. degree in electrical engineering from the Brunel University, Uxbridge, U. K., in 1998. He is currently a Professor with the College of Electrical Engineering, Sichuan University, Chengdu, China. He is the Director of the Sichuan Province Key Smart Grid Laboratory. His research interests include power system planning, operation, electricity market, artificial intelligence, and computer applications.